# COMPARISON OF LOW- AND HIGH TEMPERATURE DIFFERENTIAL STIRLING ENGINES

S. IWAMOTO[*1], F. TODA[*1], K. HIRATA[*1]
M. TAKEUCHI[*2] and T. YAMAMOTO[*3]

[*1]Department of Mechanical Engineering, Faculty of Engineering, Saitama University, Japan
[*2]Suction Gas Engine MFG. Co., Ltd., Japan
[*3]National Institute for Research and Environment, Japan

## ABSTRACT

Stirling engines can be operated with various heat sources. We have developed several Stirling engines, included a low temperature differential Stirling engine using hot spring heat and a high temperature differential Stirling engine using a combustion gas as the fuel. These engines have different features and characteristics, and have different thermal performance.

In this paper, the performances of these difference types of Stirling engines were measured, were compared using the normalized values.

## INTRODUCTION

In the field of the low temperature differential Stirling engines, several small Stirling engines have developed by I. Kolin, J. R. Senft and so on[1),2)]. We have being developed the low temperature differential Stirling engine with several hundreds wattage of an output power[3)]. The engine uses hot spring heat or hot water from industrial waste heat as the fuel.

In this paper, we measured heat losses and powers of the engine in order to estimate the engine performance. Then the performance of a prototype of the low temperature differential Stirling engine (LDSE) was compared with that of a high temperature differential Stirling engine (HDSE) after their experimental results had been normalized.
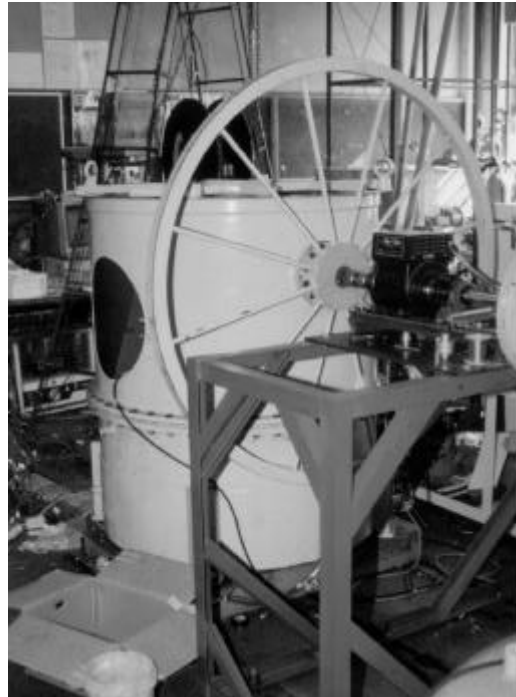


Figure 1    Feature of LDSE

# STRUCTURE OF LDSE

Figure 1 and Fig. 2 show the features and structure of LDSE. Table 1 shows specifications of this engine and HDSE[5)] used to compare the performances.

LDSE uses a gamma-type configuration, because this type engine can keep a large heat transfer area of heat exchangers. The crank mechanism is covered with a buffer tank, and the engine can be pressurized above atmospheric pressure.

The heat exchanger is located around the displacer cylinder as shown in Fig. 2. The heater and the cooler are fin-tube type heat exchangers. The hot water flows in the heater tubes. The cooling water flows in the cooler tubes. The working gas flows out of these tubes.

The crank mechanism of the power piston is a rotated Scotch-Yoke mechanism. This mechanism makes the crank assembly compact and decreases the side force on the power piston. The crank mechanism of the displacer piston uses a normal type crank mechanism. These mechanisms don't use any lubricating devices like an oil pump. The lubricant for the mechanism is only grease in the bearings. An one-way-type piston ring, which has being developed in our laboratory is used as the seal device on the power piston[4)].

It has the same effect as a pump, and a mean pressure in the working space is kept higher than the buffer space pressure. It is a suitable seal device for the low temperature difference Stirling engines, because it has low leakage of the working gas and a low friction loss. Two one-way-type rod seals, which have the same construction are used as the seal devices on the displacer rods.
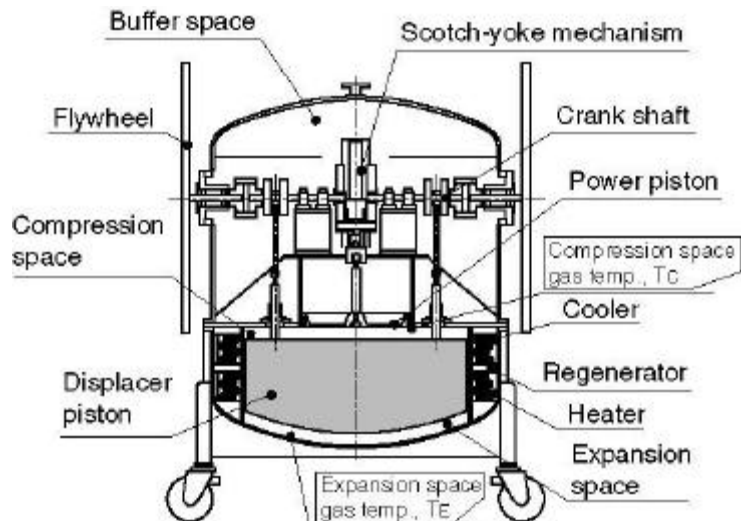


Figure 2    Schematic view of LDSE

Table 1    Specifications

|  | Low temperature difference Stirling engine (LDSE) | High temperature difference Stirling engine (HDSE) |
|---|---|---|
| Engine type | Gamma configuration | Gamma configuration |
| Power piston | | |
|    Swept volume | 25100 cm$^3$ | 81 cm$^3$ |
|    Bore / Stroke | 400 mm / 200 mm | 72 mm / 20mm |
| Displacer piston | | |
|    Swept volume | 40200 cm$^3$ | 81 cm$^3$ |
|    Bore / Stroke | 800 mm / 80 mm | 72 mm / 20mm |
| Phase angle | 90 deg | 90 deg |
| Heater type | Fin tube type | Moving tube type |
| Regenerator | | |
|    Type | Stacked mesh | Spring Mesh / Stacked mesh |
|    Material | Copper | Stainless steel |
| Cooler type | Fin tube type | Moving tube type |
| Crank mechanism | Scotch-yoke | Scotch-yoke |
| Heat source | Hot water (Hot spring) | Combustion gas |
| Working gas | Air | Helium / Air |
| Mean engine pressure | 0.1 MPa    0.3 MPa | 1 MPa |
| Expansion space temp. | 403 K | 923 K |
| Compression space temp. | 313 K (Water cooling) | 343 K (Water/Air cooling) |

# STRUCTURE OF HDSE

Figure 3 shows the structure of HDSE, which was used in the following experiments. The displacer piston of this engine has both heating and cooling inner tubes for the working gas

which flows to and from the outer tubes. A generator is located in the displacer piston.

A Scotch-Yoke mechanism is used as the crank mechanism. This keeps the crank mechanism compact. A 4-piece-type piston ring is used as the seal device of each piston. A mechanical seal is used as the seal device between the buffer space and the atmosphere.



Figure 3　Schematic view of HDSE

## ESTIMATED METHODS

Figure 4 shows a heat balance, which is discussed in this paper. This figure shows that an overall efficiency of the Stirling engine is calculated in Eq. 1 using a burner efficiency, $\eta_b$ (=$Q_{in}/Q_{total}$), an indicated efficiency, $\eta_i$ (=$L_i/Q_{in}$) and a mechanical efficiency, $\eta_m$ (=$L_s/L_i$).

$$\eta_{total} = \eta_b \times \eta_i \times \eta_m \qquad (1)$$

By the rough considerations, the burner efficiency is affected by the shape of the heat source, the indicated efficiency is affected by the heat flow in the engine, and the mechanical efficiency is affected by the mechanism and the operating conditions. The burner efficiency is difficult to consider because the engines used for this testing have different shaped heat sources. The following heats and efficiencies are based on the heat input, $Q_{in}$.

## HEATS AND LOSSES

The heat input, $Q_{in}$ is the overall heat that enters the engine. The heat input, $Q_{in}$ is calculated by Eq. 2 using indicated power, $L_i$ (measured using P-V diagrams) and rejected heat, $Q_{reject}$ as described later.

$$Q_{in} = L_i + Q_{reject} \qquad (2)$$

The expansion space power, $L_E$ is calculated by Eq. 3 using an expansion space pressure, $P_E$, a volume change of the expansion space, $dV_E$ and the engine speed, n (rps). The expansion space power, $L_E$ is measured using the overall heat that flows from the heat source to the working gas through the heater.

$$L_E = \oint P_E dV_E \cdot n \qquad (3)$$

The compression space power, $L_C$ is calculated by Eq. 4 using the compression space pressure, $P_C$ and a volume change of the
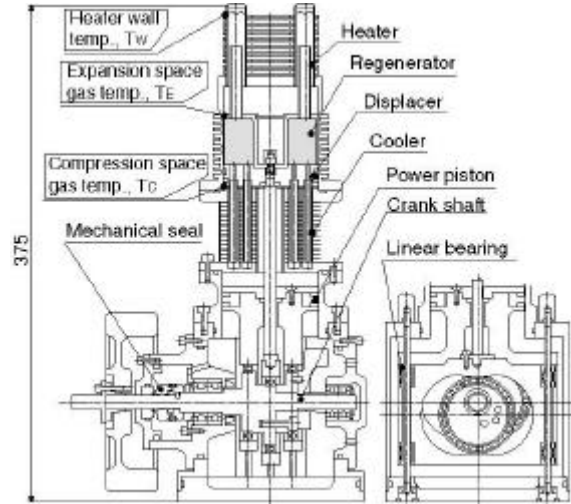


$Q_{total}$: Total heat input
$Q_{in}$: Heat input
$L_b$: Burner loss
$L_e$: Expansion space power
$Q_{other}$: Other thermal loss
$L_c$: Compression space power
$L_i$: Indicated power
$Q_{reject}$: Rejected heat
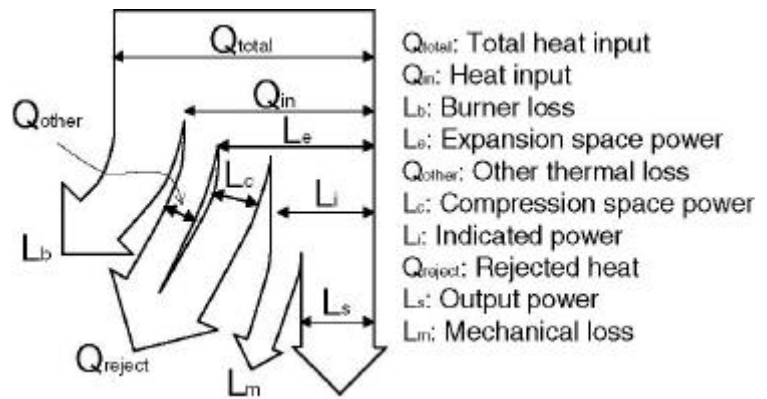$L_s$: Output power
$L_m$: Mechanical loss

Figure 4　Heat balance

compression space, $dV_C$.

$$L_C = -\oint P_C dV_C \cdot n \qquad (4)$$

The indicated power, $L_i$ is determined by the difference between $L_E$ and $L_C$ as shown in Eq. 5.

$$L_i = \oint P_E dV_E + \oint P_C dV_C = L_E - L_C \qquad (5)$$

The output power, $L_s$ is calculated by Eq. 6 using break torque, $T_q$ which was measured in the experiments.

$$L_s = 2\pi \cdot T_q \cdot n \qquad (6)$$

The rejected heat, $Q_{reject}$ is calculated by Eq. 7 using a specific heat of the cooling water, c (J/kgK), an inlet water temperature, $T_{in}$, an outlet water temperature, $T_{out}$ and a water mass flow, $m_{water}$ (kg/s).

$$Q_{reject} = c \cdot m_{water}(T_{out} - T_{in}) \qquad (7)$$

Other thermal loss, $Q_{other}$ is calculated by Eq. 8. It is considered that this loss consists mainly of a heat conduction loss and a regenerator loss.

$$Q_{other} = Q_{in} - L_e = Q_{reject} + L_c \qquad (8)$$

A pressure loss, $L_{ploss}$ is defined by Eq. 9.

$$L_{ploss} = -\oint (P_e - P_c)dV_e \cdot n \qquad (9)$$

A mechanical loss, $L_m$ is the difference between $L_i$ and $L_s$ as shown in Eq. 10.

$$L_m = L_i - L_s \qquad (10)$$

## NORMALIZED SPEED AND HEATS

In order to compare different types of Stirling engines, the engine speed and each heats should be normalized. The performances of LDSE and HDSE can be estimated directly using the normalized values.

The engine speed band is different between that of LDSE and HDSE under all operating conditions. A normalized speed, $N^*$ is defined by Eq. 11 using the engine speed, N and a rated engine speed, $N_{rate}$.

$$N^* = \frac{N}{N_{rate}} \qquad (11)$$

In the case of HDSE, the rated engine speed is set to 1000 rpm. This value is the rated speed of this design. This engine speed, 1000 rpm is the maximum permitted speed with continued safe operation. The maximum permitted speed of LDSE is higher than its power output band. In the case of LDSE, the rated engine speed, $N_{rate}$ is assumed to be set to the engine speed when it operates at the maximum output power.

In the case of the heat and losses, Q, each normalized heat, $Q^*$ is defined by Eq. 12.

$$Q^* = \frac{Q}{Q_{in}} \qquad (12)$$

## EFFICIENCIES

The indicated efficiency, $\eta_i$, the mechanical efficiency, $\eta_m$ and an internal conversion

efficiency, $\eta_{int}$ are defined by following equations.

$$\eta_i = \frac{L_i}{Q_{in}}$$ (13)

$$\eta_m = \frac{L_s}{L_i}$$ (14)

$$\eta_{int} = \frac{L_i}{L_e}$$ (15)

## EXPERIMENTAL METHODS OF LDSE

Table 2 shows experimental conditions of LDSE. The buffer pressure was maintained at atmospheric pressure (0.1 MPa) in this experiment. Ethylene glycol, maintained at a temperature of 403 K and the volume flow to 20 l/min was used as the heat source. The compression space pressure and a pressure difference between the expansion and the compression space were measured by strain gauge type sensors. Several thermocouples were used to measure temperatures. The expansion gas temperature, $T_E$ and the compression space temperature, $T_C$ were measured as representative gas temperatures at points shown in Fig. 2. The load to the engine output was adjusted by a rope break, and the engine torque, $T_q$ was measured by spring scales which were located at both ends of the rope.

Table 2   Experimental conditions of LDSE

| Heat source | Ethylene glycol |
|---|---|
| Temp. of heat source | 403 K |
| Working gas | Air |
| Buffer pressure | 0.1MPa (atmosphere) |
| Regenerator | Stacked Mesh (#24× 30 seats) |
| Cooling type | Water cooling |
| Piston ring | One-way-type |

## EXPERIMENTAL METHODS OF HDSE

Table 3 shows experimental conditions of HDSE. A mean pressure of the working space was set to 0.8 MPa. A 1 kW (max.) electric heater was used to heat the engine. Heat input from the electric heater was adjusted to maintain the heater wall temperature, $T_W$ shown in Fig. 3 to 973 K. $T_w$ indicates the highest temperature in the engine system. The expansion temperature, $T_E$ and the compression temperature $T_C$ were measured at points shown in Fig.3 using thermocouples. The load to the engine output was adjusted by changing a value of a resistance which was connected to a generator. The arm attached to the generator was connected to an electric balance to measure the engine torque, $T_q$.

Table 3   Experimental condition of HDSE

| Heat source | Electric heater |
|---|---|
| Heater wall temp. | 973 K |
| Working gas | He |
| Mean engine pressure | 0.8 MPa |
| Regenerator | Spring Mesh |
| Cooling type | Water cooling |
| Piston ring | 4-piece-type |

## EXPERIMENTAL RESULTS

ENGINE PERFORMANCE OF LDSE

Figure 5 shows the relation between the engine speed and the indicated and output power
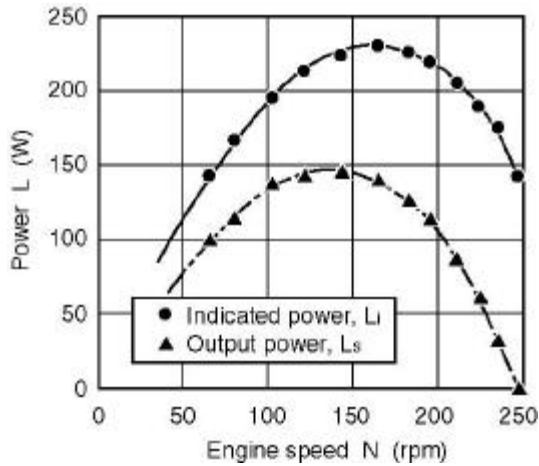
Figure 5　Power as a function of engine speed (LDSE)



Figure 6　Temperatures as a function of engine speed (LDSE)

of LDSE. This figure shows that the maximum output power reached to 146 W at the engine speed, 143 rpm. The maximum speed reached 247 rpm at no load.

Figure 6 shows the relation between the engine speed and the expansion and compression temperatures, $T_E$ and $T_C$. These values of the temperatures changed somewhat by changing the engine speed. $T_E$ was 381 K and $T_C$ was 313 K at the rated engine speed, 143 rpm.

Figure 7 shows the relation between the engine speed and the heat input, $Q_{in}$, which is determined in Eq. 2. From this figure, the heat input increases proportionally with higher engine speed.



Figure 7　Heat input as a function of engine speed (LDSE)

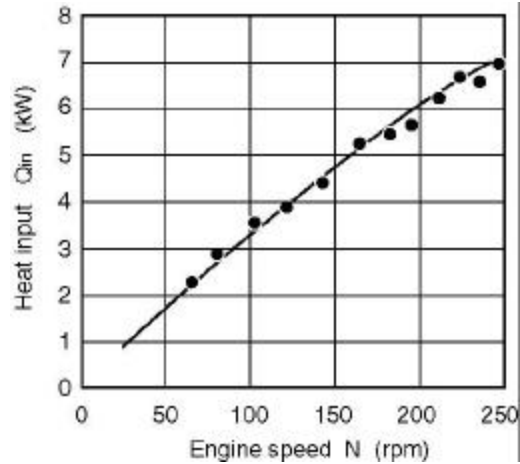ENGINE PERFORMANCE OF HDSE

Figure 8 shows the relation between the engine speed and the indicated and output power of HDSE. In the HDSE, the maximum points of the indicated and output power cannot be seen. In this experiment, the gas temperatures were not affected by the engine speed hardly, and $T_E$ was about 733 K and $T_C$ was about 309 K.

Figure 9 shows the relation between the engine speed and the heat input, $Q_{in}$, which is led to Eq. 2. From this figure, the heat input increases proportionally with higher engine speed too.
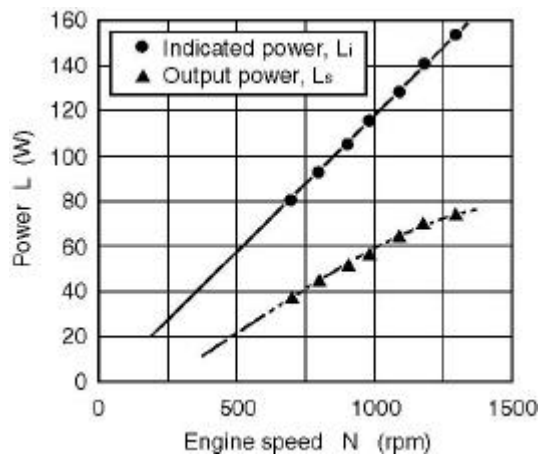


Figure 8　Power as a function of engine speed (HDSE)

## NORMALIZED HEATS

Figure 10 shows the relation between the normalized speed, $N^*$ and the normalized expansion and compression power, $L_E^*$, $L_C^*$. From this figure, $L_E^*$ of LDSE converged to that of HDSE. It means that the heat input flows to the working gas with the same rates. On the other hand, $L_C^*$ of LDSE was higher than that of HDSE. It means that the heat input of LDSE is used in order to cool the working gas with a larger rate than that of HDSE.

Figure 11 shows the relation between the normalized speed, $N^*$ and the normalized rejected and other heats, $Q_{reject}^*$ and $Q_{other}^*$. From this figure, $Q_{reject}^*$ of LDSE is higher than that of HDSE, and reaches 0.95 at the rated engine speed. $Q_{reject}^*$ of LDSE increases with higher engine speed, though that of HDSE decreases with higher engine speed. It means that LDSE doesn't use the heat input effectively at the high engine speed band. And a next subject of LDSE is how it uses the heat input effectively.

$Q_{other}^*$ of LDSE converged to that of HDSE, and their values are about 0.5. As described above, $Q_{other}$ is mainly the heat conduction loss and the regenerator loss, but accounting for these losses and these heats in this experiment was difficult. A detailed accounting of these losses is needed.

Figure 12 shows the relation between the normalized speed, $N^*$ and the normalized pressure loss, $L_{ploss}^*$. In this figure, $L_{ploss}^*$ of LDSE is lower than that of HDSE somewhat. The pressure loss and the mechanical loss in the LDSE determine the engine speed band. A way to decrease these losses should be considered.
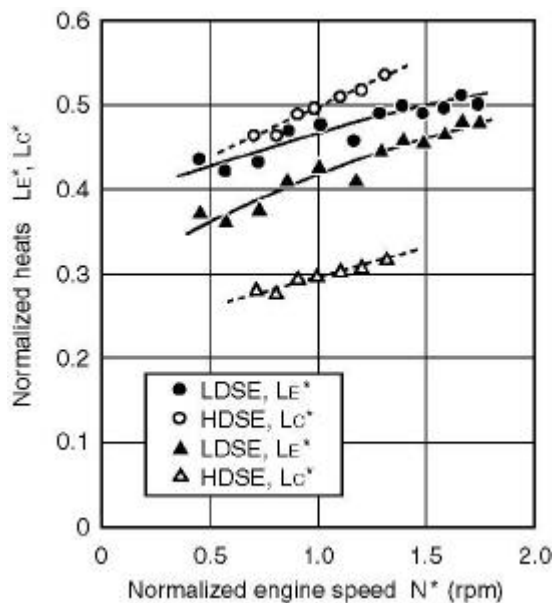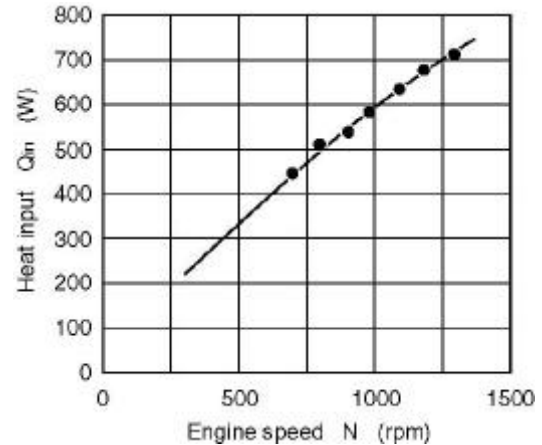


Figure 9    Heat input as a function of engine speed (HDSE)



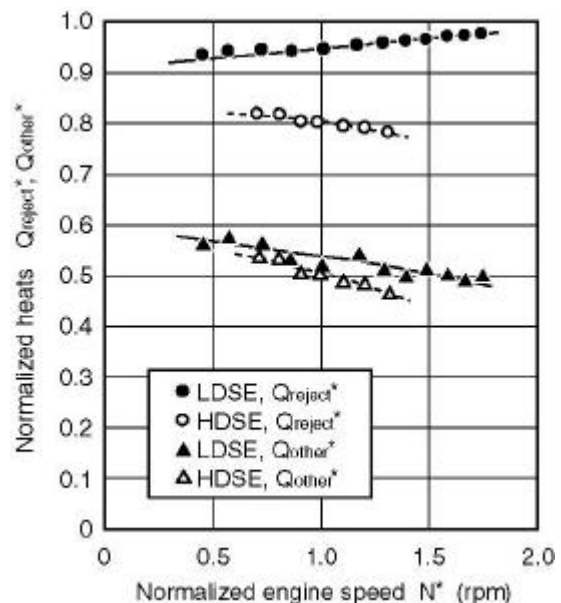Figure 10    Normalized heats as a function of normalized speed



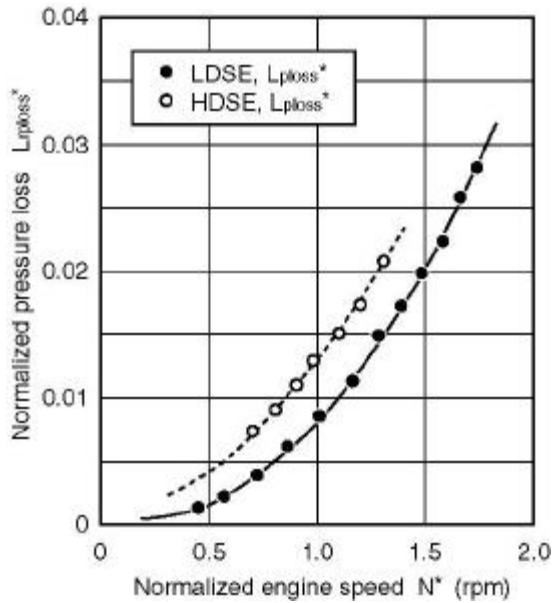Figure 11    Normalized heats as a function of normalized speed

Figure 12   Normalized pressure loss as a
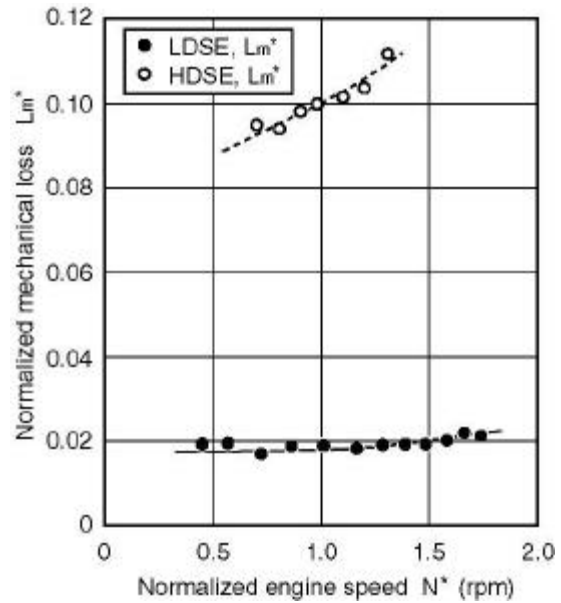function of normalized speed



Figure 13   Normalized mechanical loss as a
function of normalized speed

Figure 13 shows the relation between the normalized speed, $N^*$ and the normalized mechanical loss, $L_m^*$. In this figure, $L_m^*$ of LDSE is much lower than that of HDSE. $L_m^*$ of HDSE increases with higher engine speed, but that of LDSE keeps constant value without the effect of the engine speed. This is one of the characteristics of LDSE, which operates in the low engine speed band.


EFFICIENCIES

Figure 14 shows the relation between the normalized speed, $N^*$ and the indicated efficiency, $\eta_i$. This figure shows that $\eta_i$ of LDSE is 0.05 and that of HDSE is 0.2 at the rated engine speeds. The difference between that of LDSE and HDSE is explained clearly with a consideration of a theoretical efficiency (Carnot efficiency) which is determined by the gas temperature ratio. The indicated efficiency can be increased by decreasing the other thermal losses, $Q_{other}$.

Figure 15 shows the relation between the normalized speed, $N^*$ and the mechanical efficiency, $\eta_m$. It is difficult to compare these experimental results directly, because these engines are designed for experimental use. The mechanical efficiency, $\eta_m$ of LDSE can be increased easily, because it operates at a low
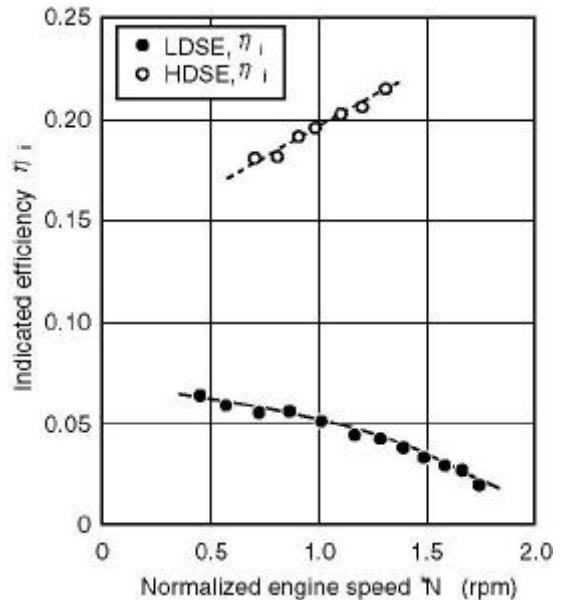


Figure 14   Indicated efficiency as a function
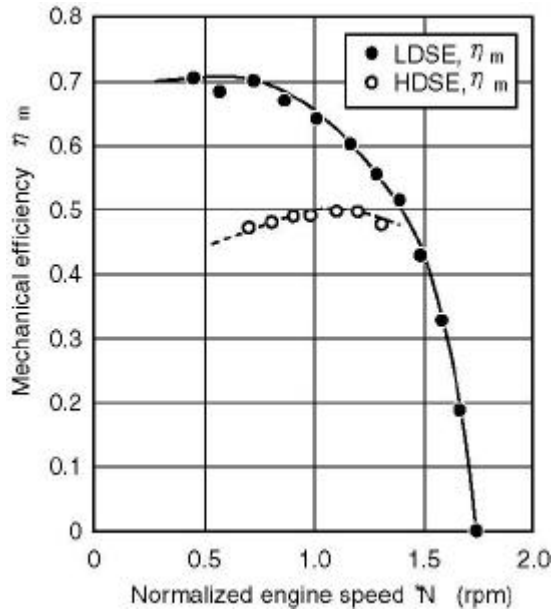of normalized speed

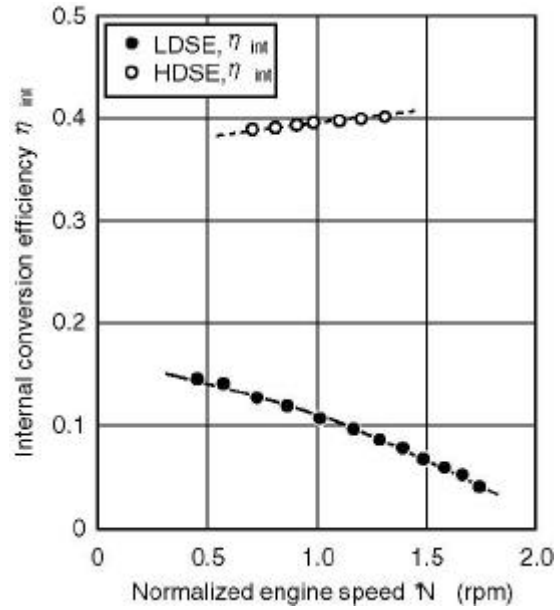Figure 15    Mechanical efficiency as a function of normalized speed



Figure 16    Internal conversion efficiency as a function of normalized speed

engine speed. It is one of the good characteristics of LDSE.

Figure 16 shows the relation between the normalized speed, $N^*$ and the internal conversion efficiency, $\eta_{int}$. The value of this efficiency is affected by that of the Carnot efficiency. The Carnot efficiency ($=1-T_C/T_E$) of LDSE is calculated to 0.20 using the expansion and compression space gas temperatures, $T_E$ and $T_C$ at the rated engine speed. That of HDSE is calculated to 0.58 with the same condition. This figure shows that of LDSE is about 50% of the Carnot efficiency at the rated engine speed. The internal conversion efficiency, $\eta_{int}$ of LDSE can be increased by the decrease of the pressure loss.


CONCLUSION


The difference types of Stirling engines are compared. The summary of the experimental and estimated results is shown below.
(1) LDSE reached 145 W of output power at the engine speed, 142 rpm and the buffer pressure, 0.1 MPa using 403 K of the heat source temperature.
(2)        The indicated efficiency of LDSE reached to 0.05, when it operated at the maximum output power.
(3) The heat input of LDSE is used in order to cool the working gas with a larger rate than that of HDSE. And the normalized rejected heat of LDSE was higher than that of HDSE. A subject for further research on LDSE is how it uses the heat input effectively.


The Carnot thermal efficiency of the low temperature differential Stirling engine will not reach that of the high temperature differential Stirling engine. But the low temperature differential Stirling engine can use many different kinds of heat sources effectively. It needs to be developed more. We will have developed it using the above experimental results.

## ACKNOWLEGEMENT

## REFFERENCE

1) Kolin, I, 1991, "Stirling Engine with Alternative Sources", Proceedings of 5th ISEC, p.421.
2) Senft, J. R., 1991, "An Ultra Low Temperature Differential Stirling Engine", Proceedings of 5th ISEC, Appendix, p.1.
3) Toda, F., et al., 1995, "Development of 300W Class Low Temperature differential Stirling Engine, Proceedings", 7th ICSC, Tokyo, JSME, p.211.
4) Toda, F., et al., 1989, "Performance Characteristics for Experimental Small Stirling Engine - Engine Performance with New Type Piston Ring-", Journal of the MESJ, Vol.24, No.6, p.150 (in Japanese).
5) Kagawa, N., et al., 1995, "Design of A 100 W Stirling Engine", Proceedings, 7th ICSC, Tokyo, JSME, p.211.
6) Hirata, K., et al., 1996, "Test Results of Applicative 100 W Stirling Engine", Proceedings, 31st IECEC, vol.2, p.1259-1264.